Supporting information for

New insights in single-step hydrodeoxygenation of glycerol to propylene by coupling rational catalyst design with systematic analysis

M. El Doukkali,[(*),1,2] F. Dumeignil,[1] S. Paul[1]

[1]*Univ. Lille, CNRS, Centrale Lille, Univ. Artois, UMR 8181, UCCS, Unité de Catalyse et Chimie du Solide, F-59000 Lille, France*

[2] *University of Sultan Moulay Slimane, Multidisciplinary Faculty of Beni-Mellal, Department of Chemistry, Av. Mghila, BP 592, 23000, Beni-Mellal, Morocco*

(*****) Corresponding author. Tel.: (+212) 671 88 06 35; Fax: (+33) 03 20 43 65 61

Email address: m.eldoukkali@usms.ma (M. El Doukkali)

Table S 1. List of all the reagents used in the preparation, characterization and tests of catalysts

Name or formula, quality and origin of reagent	Role
Tetraethylorthosilicate [$Si(OC_2H_5)_4$, 99%], Alfa-Aesar	Silica source
Poly(ethyleneoxide)-block-poly(propyleneoxide)-blockpoly (ethyleneoxide)-block [$EO_{20}PO_{70}EO_{20}$, $M_n \approx 5800$], Sigma-Aldrich	Structure directing agent
Hexadecyltrimethyl-ammonium bromide [$C_{19}H_{42}BrN$, 99%], Alfa-Aesar	Cationic surfactant
Hydrochloric acid [HCl, 37.5 %], Sigma-Aldrich	pH adjusting agent
Ammonium hydroxide [NH_4OH, 28-30 %], Sigma-Aldrich	pH adjusting agent
Phosphomolybdic Acid [$H_3[P(Mo_3O_{10})_4].12H_2O$, 99.5%], Acros Organic	Molybdenum source
Hydrofluoric acid [HF, 48%], Sigma-Aldrich	Leaching agent
Nitric acid [HNO_3, 65-67 %], Sigma-Aldrich	Leaching agent
Iron nitrate nona-hydrate [$Fe(NO_3)_3.9H_2O$, 99.5 %], ACS reagent	Iron source
Activated carbon [DARCO@KB-G, 1405.3 m^2/g], Sigma-Aldrich	Support
Methane [CH_4, 99.998 %], Air Liquide Industry	Carbon source
Propane [C_3H_8, 99.998 %], Air Liquide Industry	Carbon source
Helium [He, 99.999 %], Air Liquide Industry	Internal standard
Nitrogen [N_2, 99.999 %], Air Liquide Industry	Atmosphere controller
Hydrogen [H_2, 99.999%], Air Liquide Industry	Reactant
Oxygen [O_2/N_2, 1 %], Air Liquide Industry	Passivation agent
Ammonium [NH_3/He, 5 %], Air Liquide Industry	Acidity titration agent
Monoxide carbon [CO, 99.999%], Air Liquide Industry	Redox titration agent
C_4H_8 (1.02%), C_3H_6 (0.98%), C_2H_4 (1.04%), He (1.03%), H_2 (1.05%), CO_2 (2%), CO (1.96), N_2, (balance), Air Liquide Industry	Calibration mixture
C_4H_{10} (0.99%), C_3H_8 (1.00 %), C_2H_6 (0.99%), C_2H_2(1.01%), He (1.03%), H_2 (1.06%), CO_2 (1.91%), CO (2.06), N_2, (balance), Air Liquide Industry	Calibration mixture
n-Pentane [$CH_3(CH_2)_3CH_3$, 98 %], Alfa-Aesar	Internal standard
Hydroxyacetone [$CH_3C(O)CH_2OH$, 90 %], Sigma-Aldrich	Calibration agent
Acrolein [H_2C=CH-CHO, 90 %], Sigma-Aldrich	Calibration agent
Ethylene-glycol [$C_2H_6O_2$, 99%], Sigma-Aldrich	Calibration agent
1.2-Propanediol [$C_3H_8O_2$, 99.5%], Sigma-Aldrich	Calibration agent
1.3-Propanediol [$C_3H_8O_2$, 98%], Sigma-Aldrich	Calibration agent
Allyl alcohol [C_3H_6O, 99 %], Sigma-Aldrich	Calibration agent
1-Propanol [C_3H_8O, 99.7 %], Sigma-Aldrich	Calibration agent
Propionaldehyde [C_3H_6O, 97%], Sigma-Aldrich	Calibration agent
Acetone [C_3H_6O, 99.9%], Sigma-Aldrich	Calibration agent
Propanoic acid [$C_3H_6O_2$, 99.5%], Sigma-Aldrich	Calibration agent
Acetaldehyde [C_2H_4O, 99.5%], Sigma-Aldrich	Calibration agent
Ethanol [C_2H_5OH, 99.8%], Sigma-Aldrich	Calibration agent
Methanol [CH_3OH, 99.8%], Sigma-Aldrich	Calibration agent
Glycerol [$C_3H_8O_3$, 99.5%], Alfa-Aesar	Reactant
Dezionized water [H_2O, 100%], ELGA@	Solvent

Description of the characterization procedures:

The loading of metals was determined by Inductively Coupled Plasma Optical Emission Spectroscopy (ICP-OES) using an Agilent 720-ES apparatus. Prior to analysis, 10 mg of each sample were dissolved in an acid solution [HF (250 µL), HNO_3 (1 mL) and HCl (3 mL)] and then thermally leached at 110 ºC for 2 h using a Vulcan 42S microwave (Questron-Horiba). The carbon content was quantified by CHNS technique using a Flash Smart microanalyzer (Thermo-Fisher). The sample was burned at 1200 ºC under a flow of pure O_2, while CO_2 was quantified using a thermal conductivity detector (TCD).

The depression of melting point of melt-infiltrated Mo@SBA-15 samples (without calcination) regarding that of bare $H_3P(Mo_3O_{10})_4$,$12H_2O$ salt was *in-situ* studied as function of temperature using a Deferential Scanning Calorimetry-DSC (SETARAM). The instrument was calibrated with a certified Indium sample hermetically sealed in Al pans (~40 µL). It allowed quantifying the heat-flow corresponding to the Mo-based salt located inside the intra-pores of SBA-15 and the one which remained in the extra-pores. The experiment consists in cooling about 10 mg of each sample down to -90 °C and then to *in-situ* heat it under a flow of N_2 (50 mL(STP)/min) from -90 °C to 140 ºC (2.5 °C/min) with 15 min isothermal plateau at each extreme. The amount of extra-porous Mo salt was calculated by considering its mass melting enthalpy in each melt-infiltrated Mo@SBA-15 sample, which was compared to that of bare Mo salt; $\Delta H_m(salt) \approx 56.6$ J/g. This was done by assuming that the OMS have a negligible external surface, which does not greatly affect the degree of pore-filling. In fact, the values of mass enthalpy were measured by integrating the corresponding peaks, allowing the calculation of the amount of Mo salt (in g) in intra-pores of 1 g of SBA-15; according to eq. S1:

$$\mathrm{m(salt)}^{\text{intra-pores}}_{\text{in g/g SBA-15}} = \mathrm{m(salt)}^{\text{added}}_{\text{in g/g SBA-15}} - \mathrm{m(salt)}^{\text{extra-pores}}_{\text{in g/g SBA-15}} \qquad (\mathbf{eq.S\ 1})$$

The thermogravimetric behavior of chosen catalysts was evaluated using a TGA 2500 thermo-balance (Mettler Toledo). In each analysis, approximately 5 mg of sample was heated up to 1000 ºC (5 ºC/min) under 50 mL (STP)/min of O_2/N_2 (20/80 vol. %).

The textural properties were measured by N_2 adsorption/desorption at 77 K using a Tristar-3020 Analyzer (Micromeritics). Around 80 mg of each sample were outgassed under 3.10^{-5} Torr at 250 ºC, and then the isotherms were recorded. The specific areas were calculated using BET method (P/P_0 = 0.05–0.25). The total volume of pores (V_p(tot)) was estimated at P/P_0=0.95, while the diameter of large and narrow pores (D_p) and the distribution of pore sizes were assessed using the BJH model (desorption data) that has proved to provide reliable results for mesoporous materials.[1], [2] The volume of micropore (V_μ) was calculated by the "*t-plot*" method.

Acid-sites quantity was evaluated by NH_3-Temperature-Programmed Desorption (NH_3-TPD) using AutoChem II apparatus (Micromeritics). The post-reaction samples were analyzed in their passivated state, while fresh samples were *in-situ* reduced under similar conditions to those used in the catalytic tests (described

below in section 2.4). After degassing (~50 mg) at 115 ºC for 30 min, the sample was saturated with NH_3/He (10/90 vol. %) for 30 min, and then purged again with He for another 2 h. Finally, TPD diagram was recorded by heating up to 700 ºC (10 ºC/min), where the desorbed NH_3 was continuously monitored using TC and MS detectors.

The redox-sites were quality-and quantitatively assessed by *in-situ* CO-Infrared analysis (CO-IR) using Nicolet iS50 spectrometer. Chosen samples were compressed into fine self-supporting disc (~10 mg.cm^{-2}) and *in-situ* reduced under 30 mbar of H_2 at 500 ºC for 3 h. Then, the sample was hot evacuated at 10^{-7} mbar overnight to remove any H_2 and/or H_2O traces. Subsequently, the system was cooled under vacuum down to 100 K, and increased pressures of ultra-purified CO was progressively dosed until the equilibrium. At every injection, an IR spectrum was immediately collected in the region of 4000–1000 cm^{-1} using a resolution of 4 cm^{-1} and 64 scans. An isotherm of CO coverages was obtained by deconvoluting the vibration bands corresponding to CO chemisorption on Mo sites, as reported by Travert *et al.*[3] The population of redox-sites was taken as equivalent to CO uptake per gram of Mo in each sample; $\mathrm{mmol(CO)/g}_{Mo}$, assuming that: *i)* CO is chemisorbed as for group VIII and noble metals[4],[5] and *ii)* SiO_2 is chemically inert towards CO.[3], [6]

The crystallinity and existing phases in the catalysts were evaluated by wide-angle X-ray diffraction (XRD) using two complementary apparatus: Bruker D8 for ambient analysis, and Siemens D5000 (equipped with Anton Paar XRK900 reactor) for *in-situ* analysis. Both instruments were operated with Cu-Kα radiation (λ= 1.54 Å) and a secondary monochromator beam, which allows detecting crystalized particles up to 2 nm. The corresponding diagrams were recorded in the 2θ range of 10 to 70° using an acquisition time of 0.0 14°/s. The diameter of crystallites was estimated by Scherrer model (eq. S2):

$$\mathrm{D} = \frac{\mathrm{K}.\lambda}{\sqrt{(\beta^2 - \mathrm{S}^2)}.\cos(\theta_\beta)} \qquad (\mathbf{eq.S\ 2})$$

where D is the apparent crystallite size, K is a constant (0.89 for spherical geometry), λ is the wavelength of Cu-Kα radiation, S is the instrument line broadening corrected with a LaB_6 reference, β is the peak width at half-height intensity (FWHM), and θ_β is the Bragg-angle corresponding to the maximum intensity of the peak.

The effective incorporation of Mo inside SBA-15 pores was also confirmed by small-angle X-ray scattering (SAXS) using SMARTLAB diffractometer. This instrument is equipped with a rotating anode, multi-circles, a point/1D detector, parabolic mirror and monochromators for very high-resolution. The diffractograms were collected over powder samples at angle values between 0.5 and 4° using a step size of 0.01°/s.

All X-ray data were processed using EVA-Fit software (v1.3-1992) backed by JCPDS database. The values of 2θ at principal peaks (hkl) were used to estimate crystallites sizes and their unit cells.

The spatial arrangement of Mo nanoparticles and the morphology of OMS were studied by High-Resolution Electron Microscopy (HRTEM) using a cutting-edge MET-EFI TITAN Themis 300. This apparatus is

equipped with a monochromator, a super-X twin windowless four quadrant silicon drift detector and a spherical probe Cs aberration corrector, which allows a spatial resolution of ~ 65 pm, including for working in STEM/EDX mode. Both fresh and used samples was ultrasonically dispersed as thin foils (~50 nm) in an epoxy resin and curing. During the data acquisitions, low intensity of beam setting was used to avoid sample modification, which correspond to probe size of ~500 pm with screen currents comprised between 50 and 100 pA. The collection angles were comprised between 50 and 200 mrad, while a semi-convergence angle of 21 mrad was set for the probe beam. The distribution of particles sizes was assessed using ImageJ software on the basis of 400-600 particles grouped from about 9-14 HAADF images, whose scaling was between 2-20 nm. The average particles size was estimated according to the eq.S3:

$$D_{p,HRTEM} = \frac{\sum_i n_i d_i^3}{\sum_i n_i d_i^2} \qquad (\mathbf{eq.S\ 3})$$

Where d_i and n_i stands the diameters of each particle located on specified range and the number of particles counted within this range, respectively.

The chemical state of Mo species and the interfacial composition of chosen fresh and used catalysts were studied by *in-situ* X-ray photoelectron spectroscopy (XPS) using a Kratos Axis Ultra-DLD instrument. This spectrometer is equipped with a mono-chromated Al-Kα dual X-ray source (1486.6 eV), a double focusing hemispherical electron analyzer (40 eV) and a resistive anode detector, which allow to scan a spot-size of 400 μm. For fresh samples, the powder was slightly pressed in a metallic-holder to be *in-situ* reduced in specific chamber operated under similar conditions to those applied during the kinetic tests. After reduction, the sample were immediately transferred to ultra-high vacuum (7.10^{-12} Torr) to avoid any contact with air. Then, the XPS spectra were recorded over an area of ≈ 1 mm^2 with 200 W x-rays at 50 eV pass energy and 0.1 eV/step. All the obtained spectra were processed using CasaXPS software by means all the binding Energy (BE) of Mo3d, C1s, Si2p, and O1s were calibrated to the BE of C1s of adventitious carbon (284.8 eV). The interfacial atomic fractions of each species were calculated by; i) normalizing the area of the corresponding peaks using the relative sensitivity factors (RSF) of Wagner for each atom (Mo, C, O and/or Si), and ii) fitting the experimental curves to the Gaussian/Lorentzian line shape of LA (1.1,2.3,2), so that each peak have the same with (FWHM). The deconvoluted peaks of $Mo3d_{5/2}$ and $Mo3d_{3/2}$ components were fixed with a shift of 3.2 eV for Mo^{6+} and Mo^{5+}, and of 3.14 eV for both Mo^{4+}, Mo^{3+} and Mo^{2+}-C. The relative area ratios of the Mo3d spin-orbit doublets were optimized so that $A(3d_{5/2})/A(3d_{3/2})$ =1.5 to comply with their respective degeneracies (2j+1). The oxidized Mo^{6+}, Mo^{5+}, Mo^{4+} and Mo^{3+} species were modeled as one set of doublets. However, the carbidic Mo^{2+}-C bands was modeled as three pairs of doublets; as recently revealed by surface science.[7], [8]

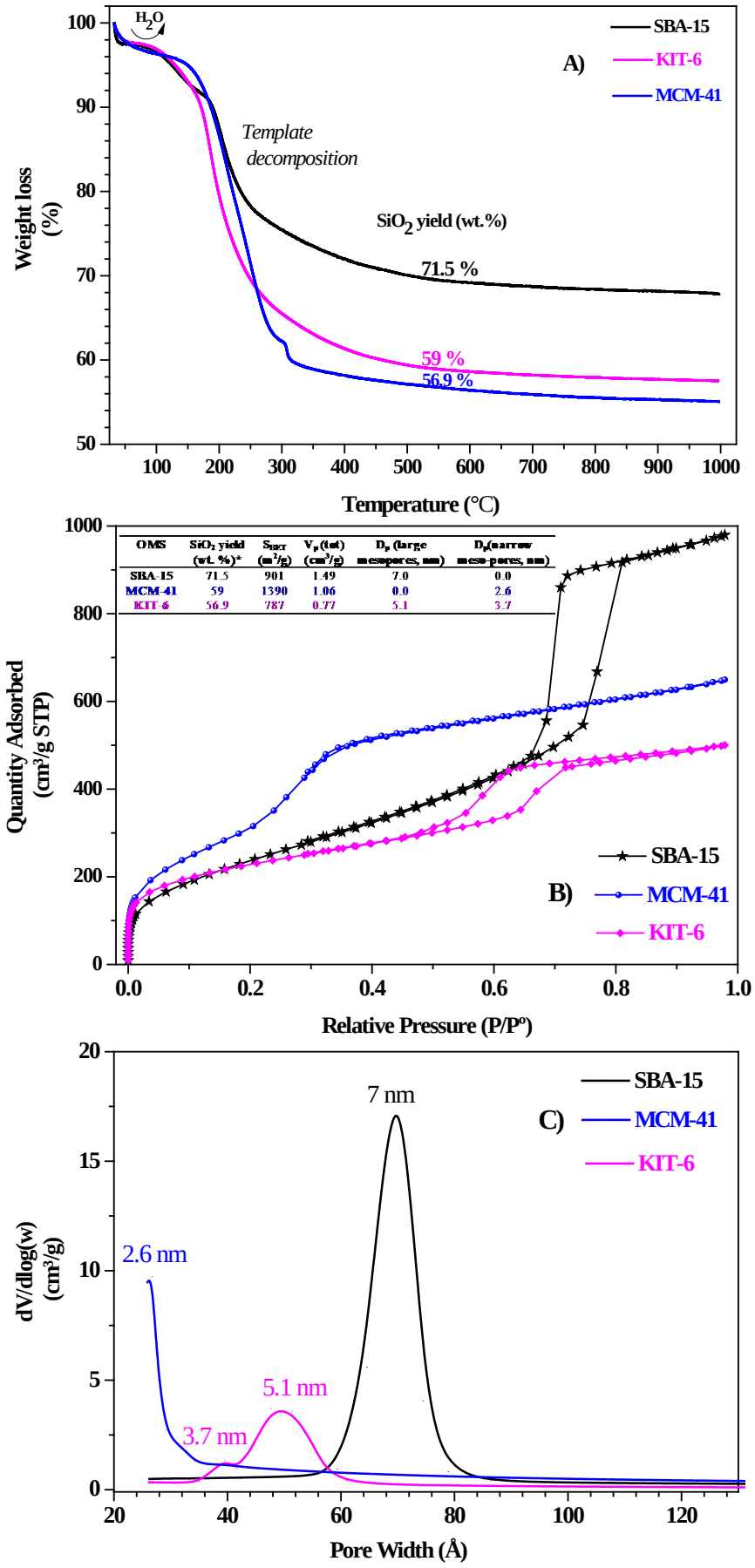

OMS	SiO_2 yield (wt. %)*	S_{BET} (m^2/g)	V_p (tot) (cm^3/g)	D_p (large mesopores, nm)	D_p (narrow mesopores, nm)
SBA-15	71.5	901	1.49	7.0	0.0
MCM-41	59	1390	1.06	0.0	2.6
KIT-6	56.9	787	0.77	5.1	3.7

Fig. S1. A) TGA profiles recorded under synthetic air to estimate the mass yield of SiO_2 for the as-synthetized SBA-15, KIT-6 and MCM-41 materials, **B)** N_2 physisorption isotherms for the bare OMS samples calcined at 500 ºC, and **C)** their BJH pore-sizes distributions.

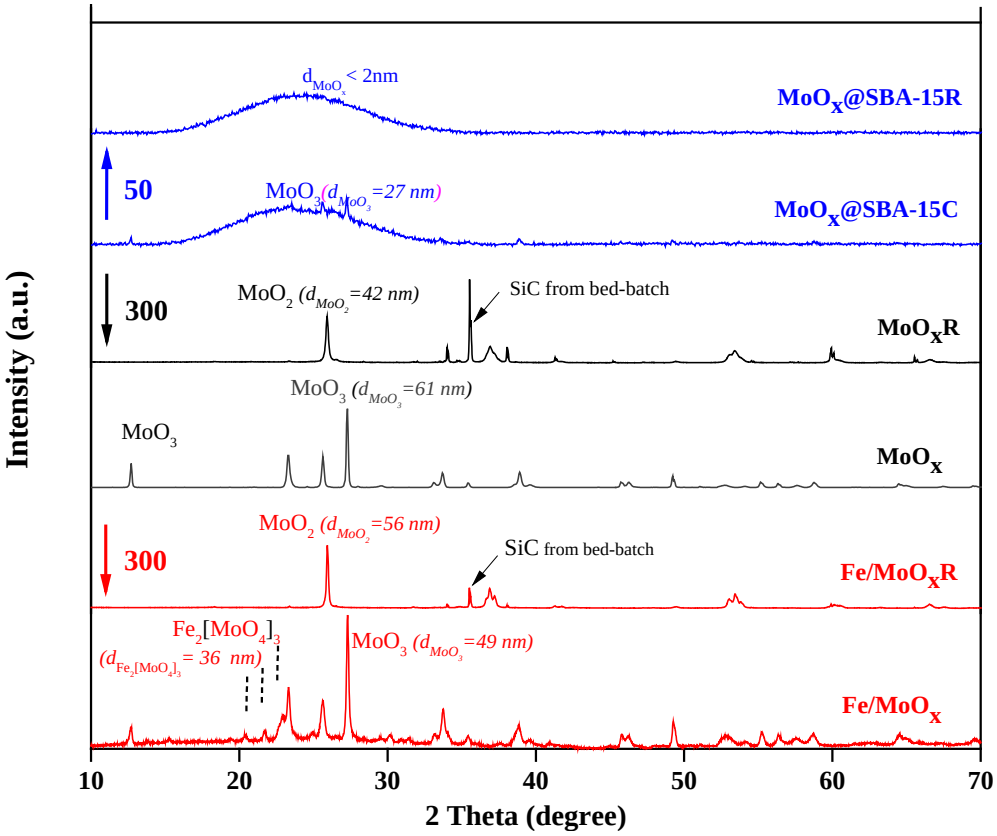

Fig. S2. XRD diagrams of calcined Fe/MoO_x and reduced Fe/MoO_xR, calcined MoO_x and reduced MoO_xR, and calcined 14.8MoO_x@SBA-15C and reduced 14.8MoO_x@SBA-15R samples.

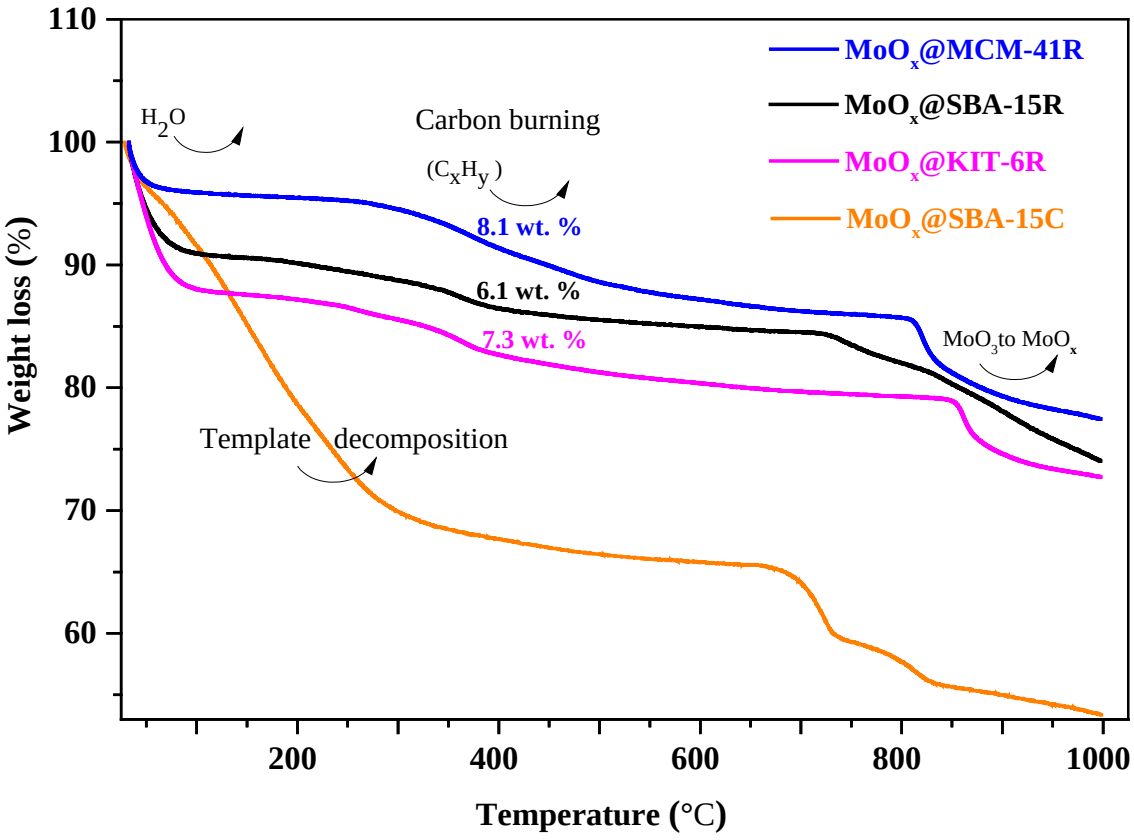

Fig. S3. TGA diagrams of as-synthetized MoO_x@SBA-15C, and of pre-reduced MoO_x@SBA-15R, MoO_x@MCM-41R and MoO_x@KIT-6R catalysts; recorded by heating from 25 ºC to 1000 ºC (5 ºC/min) under continuous-flow of synthetic O_2/N_2 mixture (20/80 vol. %).

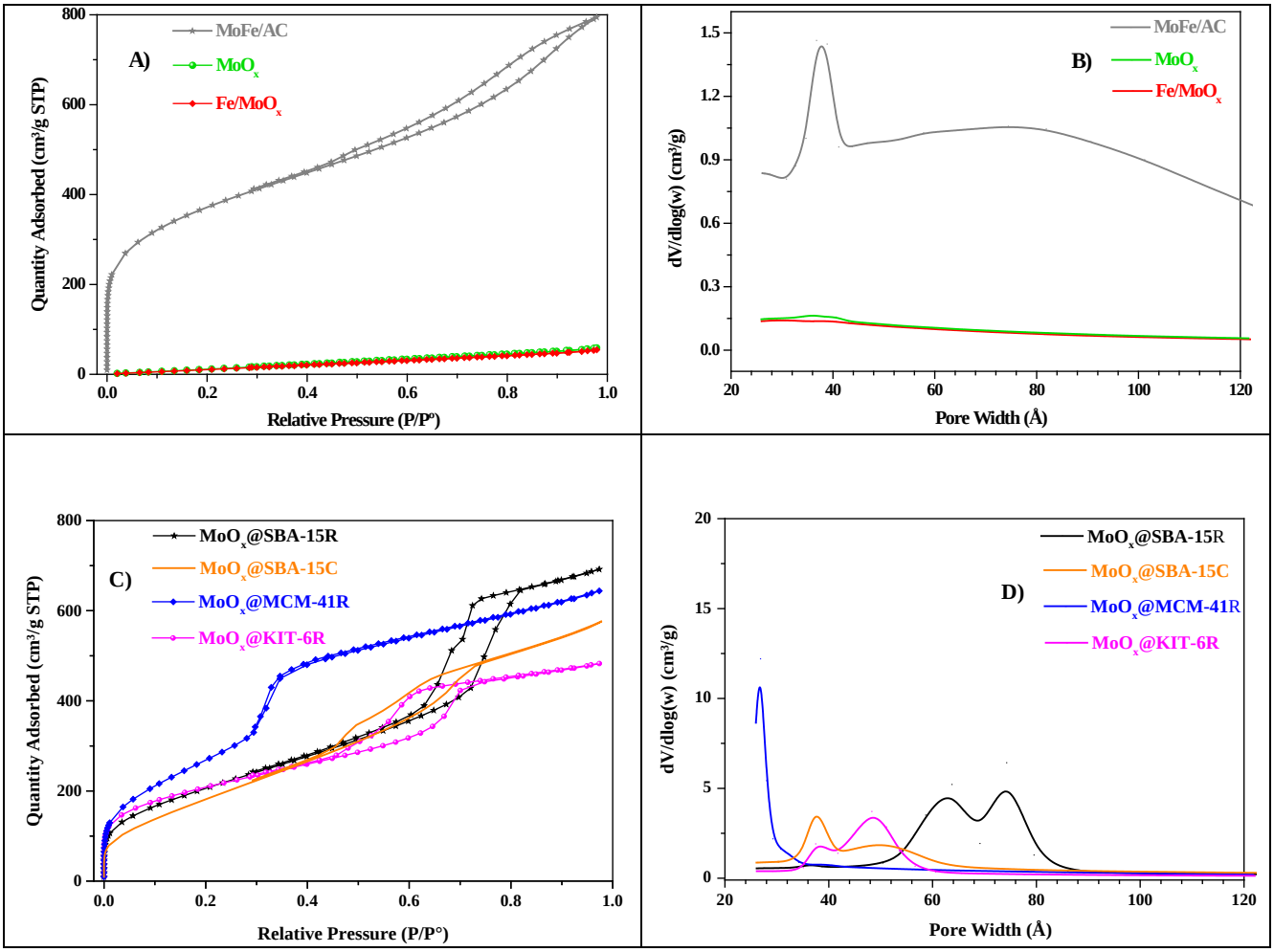

Fig. S4. N_2 physisorption isotherms (**A and C**), and BJH pore-sizes distributions (**B and D**) for pre-calcined MoFe/AC, Fe/MoO_x, MoO_x and MoO_x@SBA-15C catalysts, and for pre-reduced MoO_x@SBA-15R, MoO_x@MCM-41R, and MoO_x@KIT-6R catalysts.

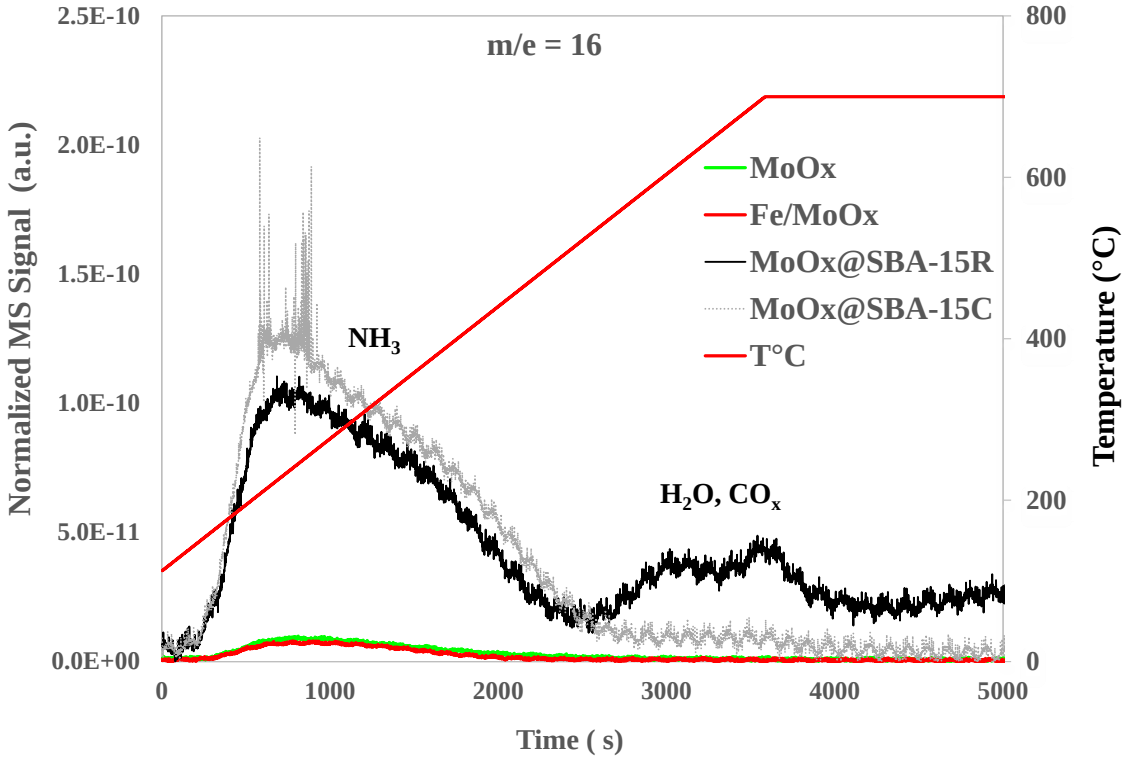

Fig. S5. Normalized NH_3-TPD profiles per 1g of Mo element for *in-situ* reduced MoO_x, Fe/MoO_x, MoO_x@SBA-15R and MoO_x@SBA-15C catalysts.

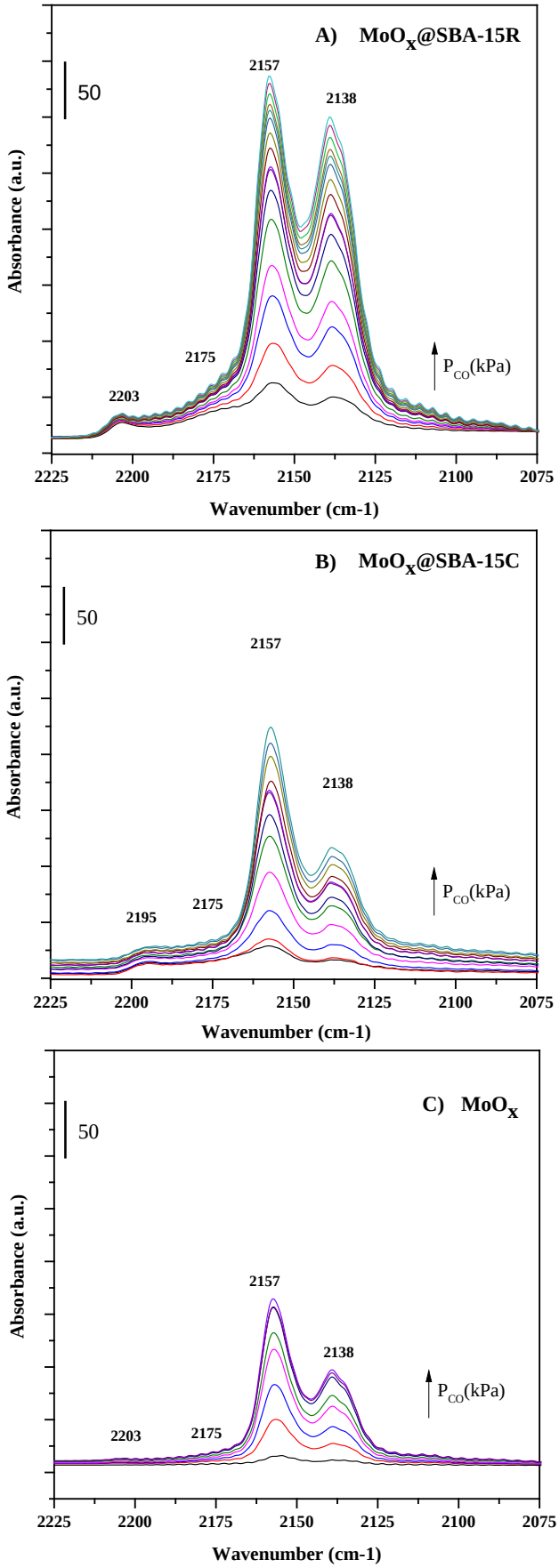

Fig. S6. Evolution of the *in-situ* FTIR spectra normalized per 1g of Mo element, and recorded under dynamic vacuum up to equilibrium of CO adsorption at 100 K over reduced MoO_x@SBA-15R **(A)** , MoO_x@SBA-15C **(B)** and bulk MoO_x **(C)**catalysts.

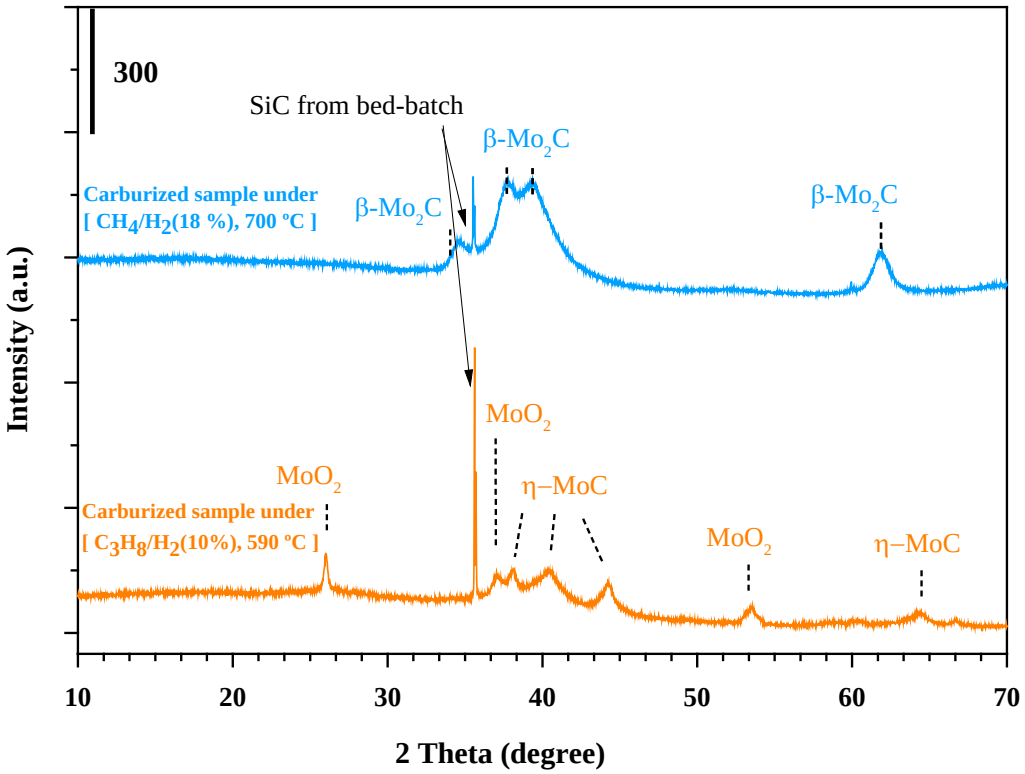

Fig. S7. XRD diagrams of fresh MoO_3 sample carburized under continuous low of CH_4/H_2 mixture (18/82 vol.%) at 700 ºC and of C_3H_8/H_2 mixture (10/90 vol.%) at 590 ºC.

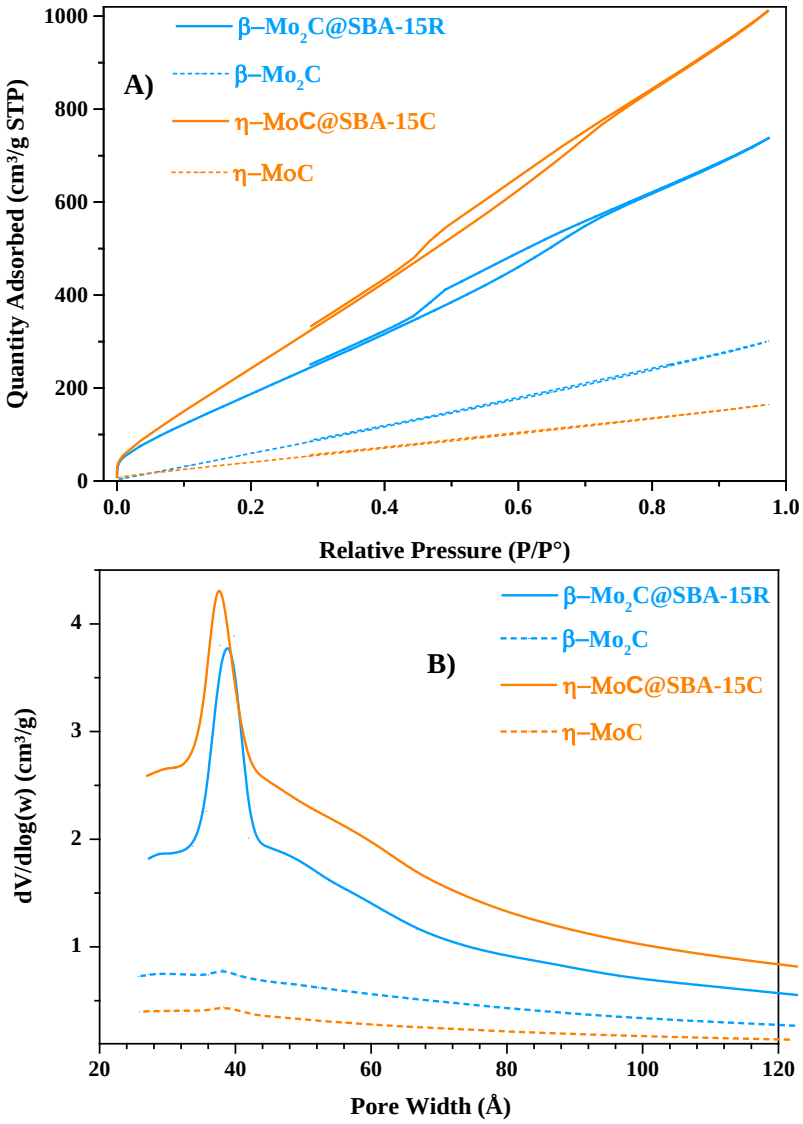

Fig. S8. A) N_2 physisorption isotherms, and **B)** BJH pore-sizes distribution for β-Mo_2C, β-Mo_2C@SBA-15R, η-MoC and η-MoC@SBA-15R catalysts.

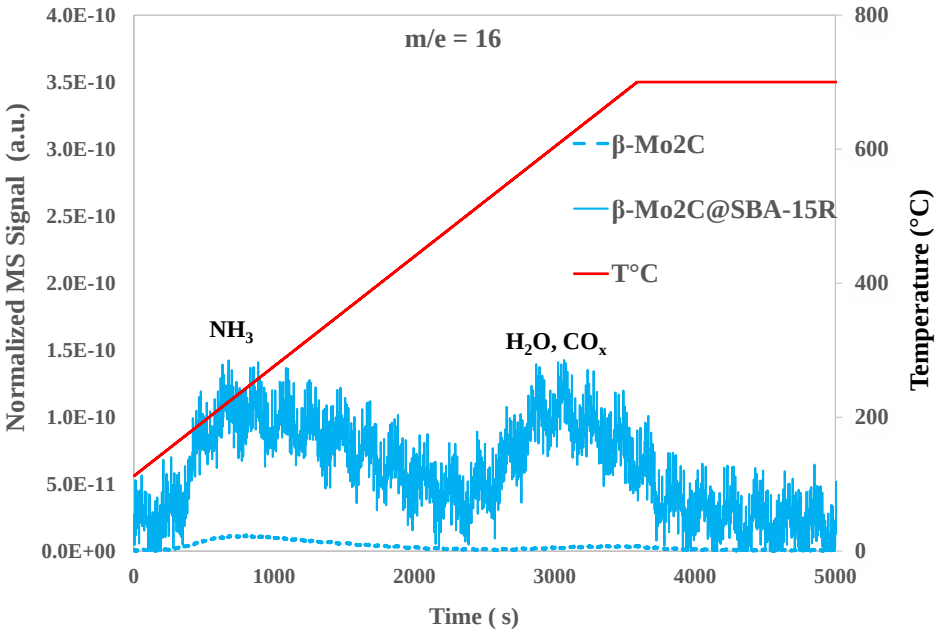

Fig. S9. Normalized NH_3-TPD profiles per 1g of Mo element for *in-situ* reduced β-Mo_2C and β-Mo_2C@SBA-15R catalysts.

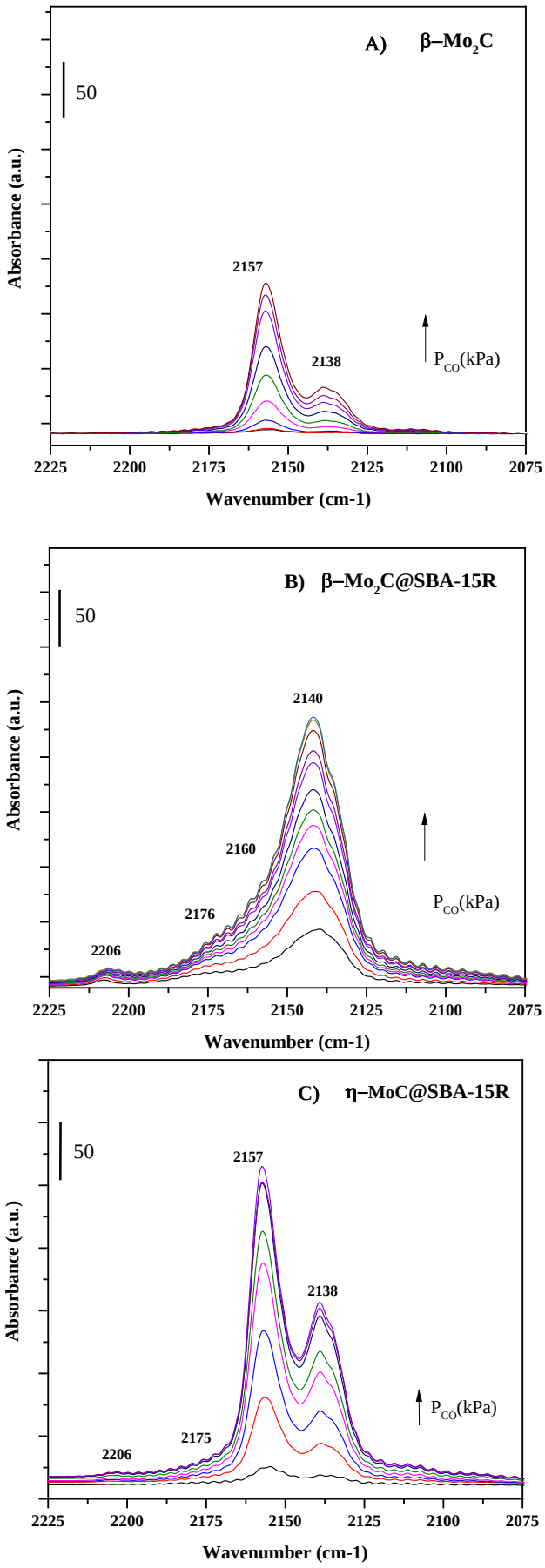

Fig. S10. Evolution of the *in-situ* FTIR spectra normalized per 1g of Mo element, and recorded under dynamic vacuum up to equilibrium of CO adsorption at 100 K over reduced β-Mo_2C (**A**), β-Mo_2C@SBA-15R (**B**) and η-MoC@SBA-15R (**C**) catalysts.

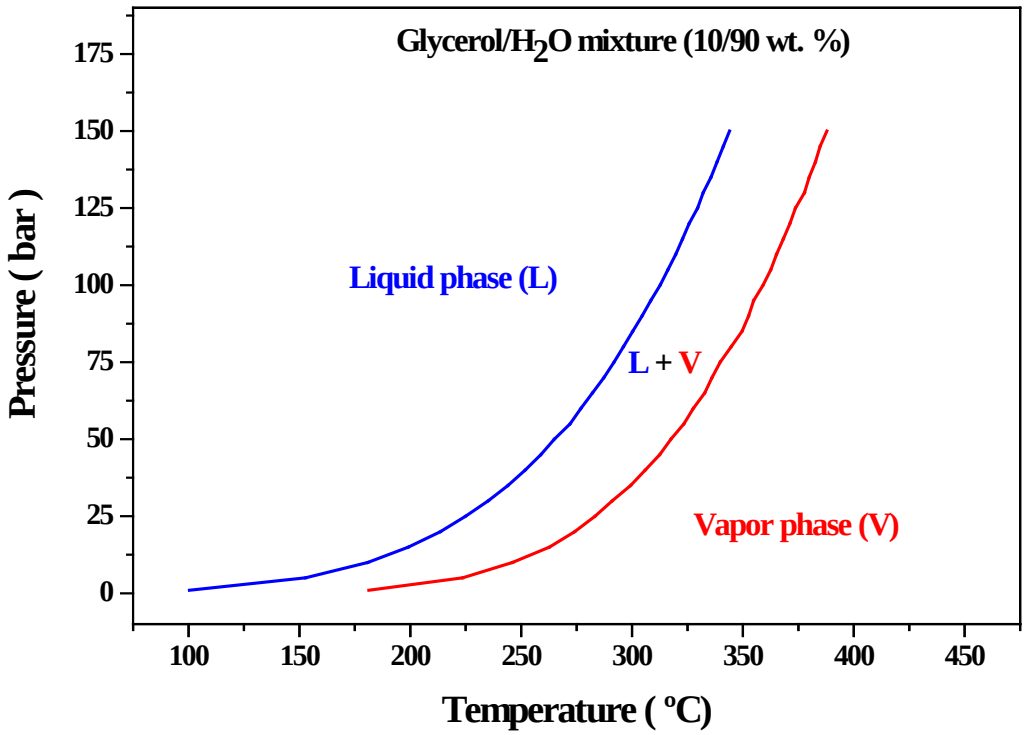

Fig. S11. Temperature and pressure limit of the existence of gas and liquid phases for an aqueous solution of glycerol (10/90 wt. %). Thermodynamic data calculated by inversing the temperature and pressure of series of binary-diagrams built at different temperature and pressure and setting the chemical weight composition at $X_{gly.} = 0.1$.

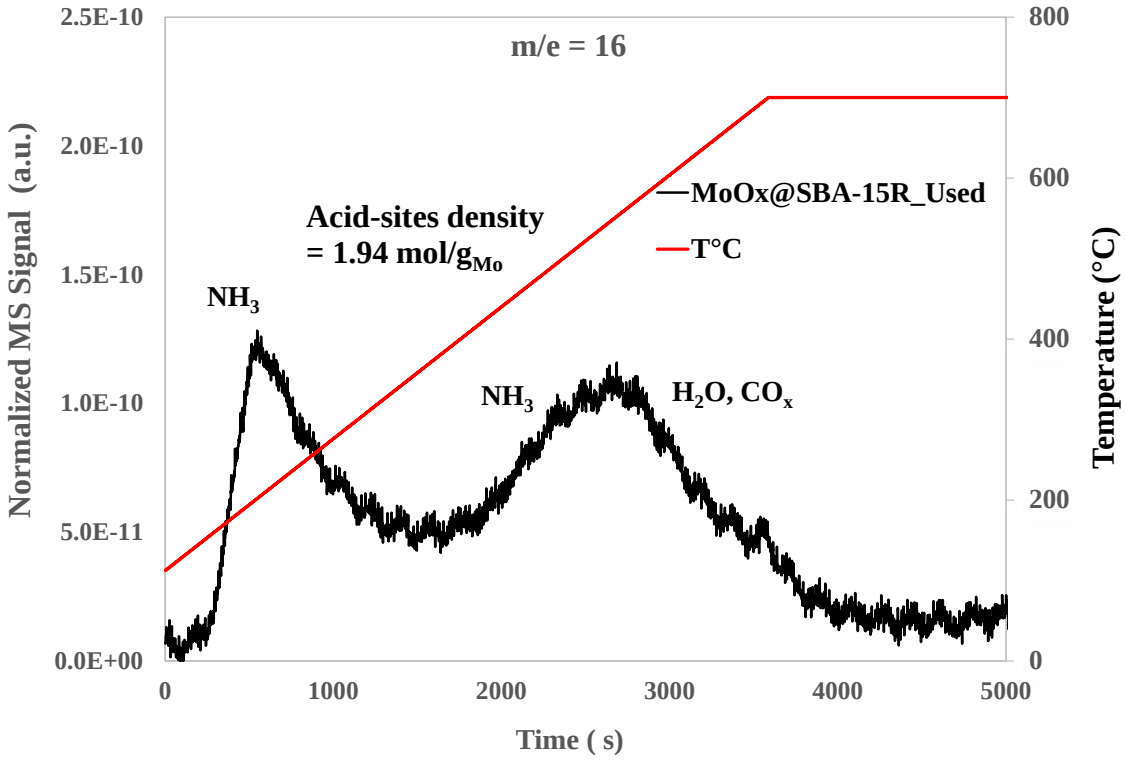

Fig. S12. Normalized NH_3-TPD profile per 1g of Mo element for used MoO_x@SBA-15R catalysts.

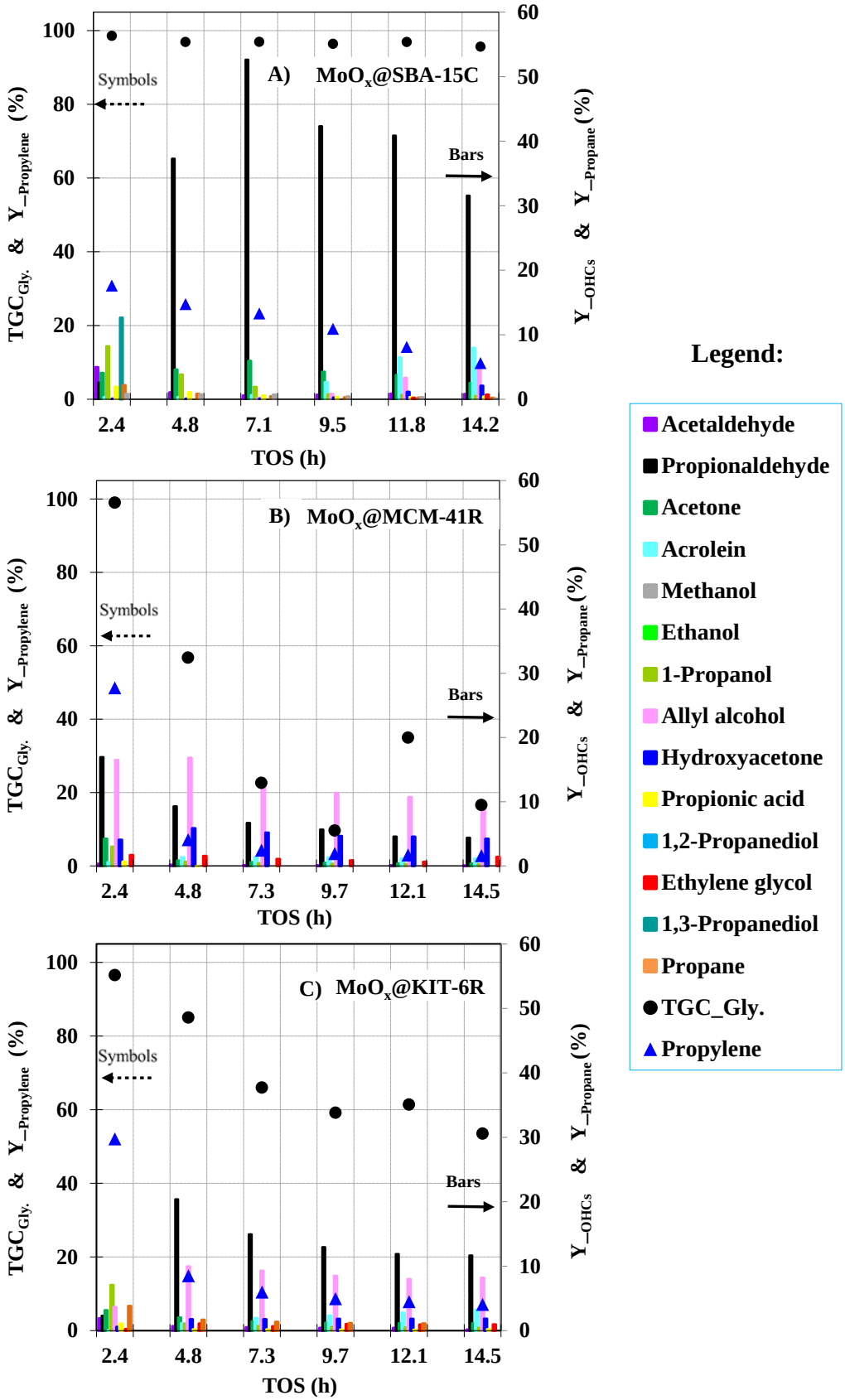

Fig. S13. Evolution of total glycerol conversion and of products yields as function of TOS for; **A**) MoO_x@SBA-15C, **B**) MoO_x@MCM-41R and **C**) MoO_x@KIT-6R catalysts, tested in single-step HDO of glycerol/water (10 wt. %) at 318 °C, 50 bar, $H_2/C_3H_8O_3$ (mol)=98 and WHSV=1.7 h^{-1}.

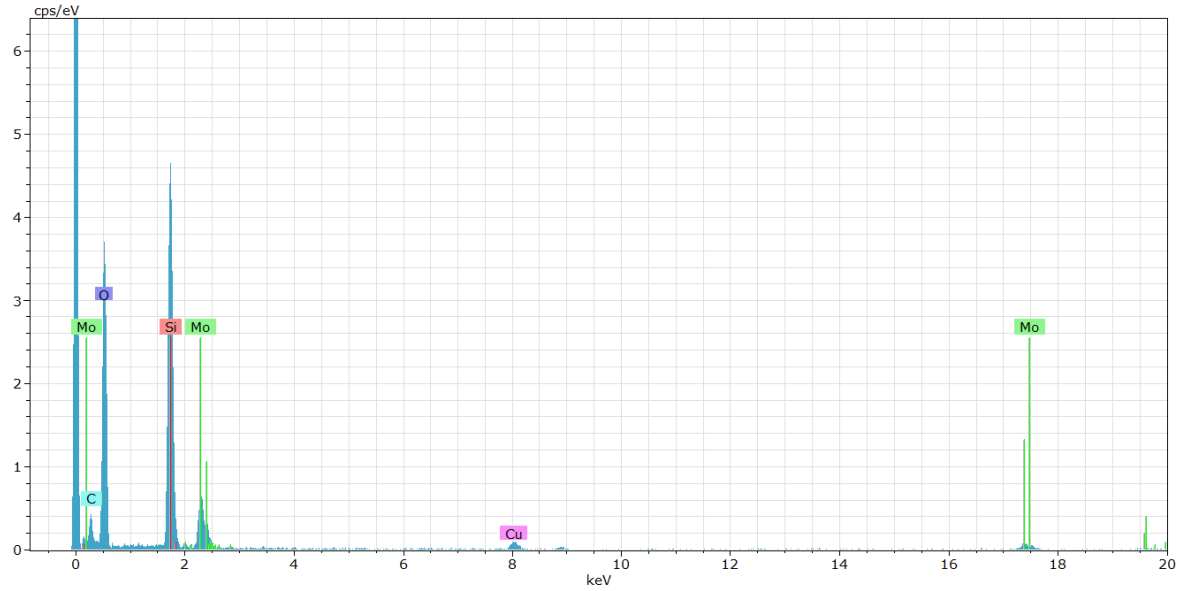

Fig. S14. EDX spectra for selected mesopores area of used β-Mo_2C@SBA-15R that reflects the intensity of Mo atomic loading regarding those of Si, O and C. The carbon signal contains also contribution of the carbonaceous resin, while Cu signal originates from the support grid used during the analysis.

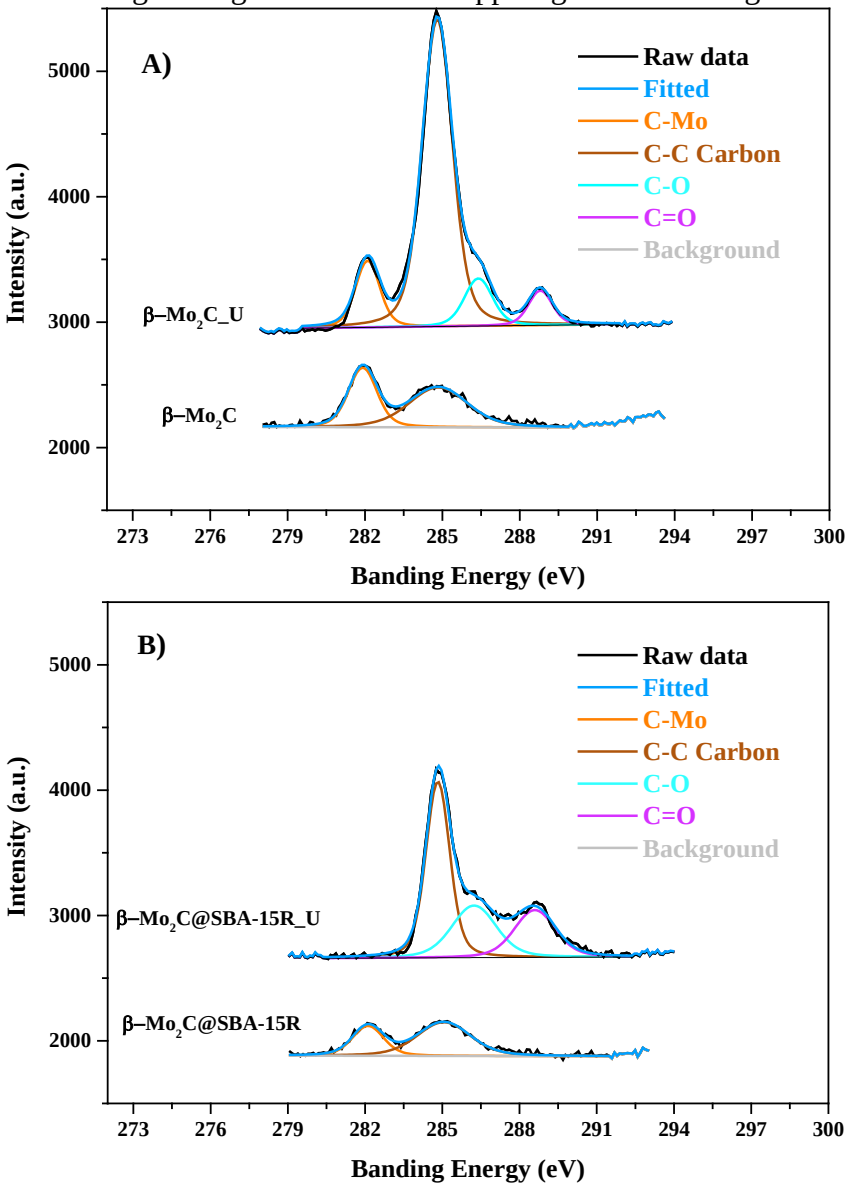

Fig. S15. XPS spectra of C1s core-level and their deconvolution for fresh and used β-Mo_2C (**A**) and β-Mo_2C@SBA-15R catalysts (**B**).

References:

[1] M. El Doukkali *et al.*, 'A comparison of sol–gel and impregnated Pt or/and Ni based γ-alumina catalysts for bioglycerol aqueous phase reforming', *Applied Catalysis B: Environmental*, vol. 125, pp. 516–529, août 2012, doi: 10.1016/j.apcatb.2012.06.024.

[2] S. K. Jana, A. Mochizuki, and S. Namba, 'Progress in Pore-Size Control of Mesoporous MCM-41 Molecular Sieve Using Surfactant Having Different Alkyl Chain Lengths and Various Organic Auxiliary Chemicals', *Catalysis Surveys from Asia*, vol. 8, no. 1, pp. 1–13, Feb. 2004, doi: 10.1023/B:CATS.0000015110.85694.d9.

[3] A. Travert *et al.*, 'Parallel between infrared characterisation and ab initio calculations of CO adsorption on sulphided Mo catalysts', *Catalysis Today*, vol. 70, no. 1, pp. 255–269, Oct. 2001, doi: 10.1016/S0920-5861(01)00422-9.

[4] J. Raskó and J. Kiss, 'Infrared study of the adsorption of CO and CH3 on silica-supported MoO3 and Mo2C catalysts', *Applied Catalysis A: General*, vol. 253, no. 2, pp. 427–436, Oct. 2003, doi: 10.1016/S0926-860X(03)00555-6.

[5] W. Wu, Z. Wu, C. Liang, X. Chen, P. Ying, and C. Li, 'In Situ FT-IR Spectroscopic Studies of CO Adsorption on Fresh Mo2C/Al2O3 Catalyst', *J. Phys. Chem. B*, vol. 107, no. 29, pp. 7088–7094, Jul. 2003, doi: 10.1021/jp027582m.

[6] V. O. O. Gonçalves *et al.*, 'Effect of the support on the hydrodeoxygenation of m-cresol over molybdenum oxide based catalysts', *Applied Catalysis B: Environmental*, vol. 214, pp. 57–66, Oct. 2017, doi: 10.1016/j.apcatb.2017.05.003.

[7] D. O. Scanlon, G. W. Watson, D. J. Payne, G. R. Atkinson, R. G. Egdell, and D. S. L. Law, 'Theoretical and Experimental Study of the Electronic Structures of MoO3 and MoO2', *J. Phys. Chem. C*, vol. 114, no. 10, pp. 4636–4645, Mar. 2010, doi: 10.1021/jp9093172.

[8] B. Frank, T. P. Cotter, M. E. Schuster, R. Schlögl, and A. Trunschke, 'Carbon Dynamics on the Molybdenum Carbide Surface during Catalytic Propane Dehydrogenation', *Chemistry – A European Journal*, vol. 19, no. 50, pp. 16938–16945, 2013, doi: 10.1002/chem.201302420.